Comput. Methods Appl. Mech. Engrg. 200 (2011) 1833–1845

Contents lists available at ScienceDirect

Comput. Methods Appl. Mech. Engrg.

journal homepage: www.elsevier.com/locate/cma

A two-steps time discretization scheme using the SPH method for shock wave propagation

M.I. Herreros [a,*], M. Mabssout [b]

[a] Escuela Técnica Superior de Ingeniería Informática, Universidad Rey Juan Carlos (URJC), Madrid, Spain
[b] Faculté des Sciences et Techniques de Tanger, Equipe Matériaux et Mécanique des Structures, BP: 416, Tanger, Morocco

ARTICLE INFO

Article history:
Received 19 September 2010
Received in revised form 16 January 2011
Accepted 4 February 2011
Available online 21 March 2011

Keywords:
TSPH
Lagrangian kernel
Dynamics
Shock wave
Shear band
Viscoplastic

ABSTRACT

The Smoothed Particle Hydrodynamics (SPH) is a meshfree method which has been applied to a wide range of problems. In the present work, a new time integration algorithm using a corrected SPH spatial discretization for small deformations is applied to solve the propagation of shock waves in viscoplastic continua. In the method presented herein the equations are formulated in terms of stress and velocity. A corrected Lagrangian kernel is employed and two different sets of particles are used for the time discretization. Numerical instabilities are not present when using this new SPH formulation. The method proposed here has been proved to be efficient and it provides solutions of good accuracy.

1. Introduction

Many numerical methods are based on computational meshes. That is the case of the Finite Difference Method, Finite Element Method and Finite Volume Method. These methods have been successfully used to solve many engineering problems in Solid and Fluid Mechanics, and many references can be found in the literature.

However, classical approaches based on a computational mesh present two important shortcomings: (i) for modelling large deformations and failure of solids, it is necessary the use of remeshing techniques if an acceptable solution is expected; (ii) for modelling free surface flows as well as dynamic fracture and fragmentation of solids, it is necessary the use of some advanced techniques such as the Level-Set algorithm [13,34] or the Extended Finite Element Method (X-FEM) [9].

To overcome these difficulties, great efforts have been devoted to develop and improve meshfree methods in the last decades. These methods can achieve numerical solutions without using any computational grid since they are based only on nodes (or particles) where field variables and their derivatives are approximated. Although most meshfree methods are Lagrangian in character, their main advantage is that the absence of a mesh enables them to deal with larger local distortion than Finite Element Methods. This flexibility has been exploited in many applications in Fluid and Solid Mechanics, such as free-surface flows, metal forming, explosion phenomena, fracture and fragmentation, to name a few [6,7,18,26,31].

One of the oldest meshfree methods is the Smoothed Particle Hydrodynamics (SPH). It is a meshfree particle method based on kernel approximations. The SPH was initially developed by Lucy [20] and Gingold and Monaghan [12,24] to simulate astrophysical problems and, in 1993, Libersky and Petschek extended SPH to Solid Mechanics [18,19]. Early SPH formulations suffered from spurious instabilities and lack of consistency that were main topics of research during the 90s, and as a consequence many corrected SPH versions were developed that improved either the stability behaviour of SPH or its consistency. Motivated by the purpose to model arbitrary crack propagation without computational expensive remeshing, Belytschko et al. developed the Element-free Galerkin (EFG) method in 1994 [3]. The EFG method is based on field approximations and it avoids inconsistencies inherent to some SPH formulations. In 1995, Liu et al. [17] proposed a similar method, the Reproducing Kernel Particle Method (RKPM) which uses a correction function that restores linear (first-order) completeness of the kernel function. Though the method is very similar to the EFG method, it originates from wavelets rather than from curve-fitting. Another very popular meshfree method that is worth mentioning is the Meshless Local Petrov Galerkin (MLPG) method

* Corresponding author. Address: Escuela Técnica Superior de Ingeniería Informática, Universidad Rey Juan Carlos, Dpto. Arquitectura de Computadores, C/ Tulipán s/n, Móstoles, Madrid, Spain.
E-mail address: isabel.herreros@urjc.es (M.I. Herreros).

0045-7825/$ - see front matter © 2011 Elsevier B.V. All rights reserved.
doi:10.1016/j.cma.2011.02.006

developed by Atluri and Shen in 1998 [1]. In this context, Atluri introduced the notion of "truly" meshfree methods since truly meshfree methods do not need a construction of a background mesh for integration.

The issue of integration in meshfree methods was another important topic of research since its early times. Methods based on a global weak form may use three different types of integration schemes: nodal integration, stress-point integration and integration based on a background mesh that does not necessarily need to be aligned with the particles. Nodal integration is, from the computational point of view, the easiest and cheapest way to build the discrete system of equations but it is similar to reduced Finite Elements. Yet meshfree methods based on nodal integration suffer from instability due to rank deficiency. Adding stress points to the nodes can eliminate (or at least reduce) this instability. The term stress-point integration comes from the fact that additional nodes are added to the particles where only stresses are evaluated. The concept of stress points was actually first introduced in a SPH setting in one dimension by Dyka and co-workers [10,11] and this concept was extended to multi-dimensional space by Randles and Libersky [32,33]. Later, Rabczuk and co-workers [29,30] developed an alternative form of stress-point integration for multi-dimensions that employs both the particles and stress points and it shows better stability properties than nodal integration.

Another important issue regarding stability of meshfree methods is related to the kernel function. This kernel function can be expressed in terms of material coordinates or spatial coordinates. It is then referred to as Lagrangian or Eulerian kernel, respectively. Early meshfree methods, such as SPH, used an Eulerian kernel. However, many meshfree methods based on Eulerian kernels suffer from a so-called tensile instability, meaning the method gets unstable when tensile stresses occur, as a result of combining an Eulerian kernel with a Lagrangian description of motion. On the contrary, meshfree methods based on Lagrangian kernels do not show this type of instability [2,29]. Nevertheless, for too large deformations, methods based on Lagrangian kernels tend to get unstable as well since the domain of influence in the current configuration can become extremely distorted. To overcome this problem, Rabczuk and Belytschko [30] proposed a method for transitioning from Lagrangian to Eulerian kernels in order to model severe deformations such as fracture and fragmentation of solids.

In the present paper, a new time discretization algorithm using SPH for solving the propagation of shock waves in viscoplastic media for small deformations is proposed. Modelling of shock waves propagation in solids is most demanding area since a wide variety of problems is encountered. The shocks are smoothed and leading or trailing oscillations appear. The situation is more involved in the non-linear regime, where strain can localize along shear bands which may be affected by the mesh if the Finite Element Method (FEM) is used in the analysis. The authors of this paper have proposed in previous works a numerical model formulated in terms of stress and velocity based on the Taylor–Galerkin scheme to solve the problem of shock waves propagation in solids using the Finite Element Method [21–23].

However, modelling of shock waves propagation in solids with SPH provides some important advantages as compared to FEM: (i) the absence of a mesh enables it to deal with larger local distortion, and (ii) mesh dependence problems such as mesh alignment or mesh size dependence, are solved in a straightforward manner given the meshfree nature of the method.

The proposed method consists of a two-steps time discretization algorithm by means of a Taylor series expansion and a corrected SPH method for the spatial discretization. The equations are formulated in terms of stress and velocity. A corrected Lagrangian kernel is employed and two different sets of particles are used for the time discretization. The purpose of the paper is to apply this new time discretization to SPH showing that the proposed method performs better than standard time discretizations used traditionally with SPH. It will be shown that numerical instabilities are eliminated when using this new SPH formulation.

The paper is arranged as follows: model equations are given in Section 2. Then, numerical discretization is presented in Section 3. Within this section, the proposed time discretization algorithm using a Lagrangian kernel and two different sets of particles is described. Finally, to assess the performance of the proposed algorithm, some numerical applications in 1D and 2D are presented in Section 4. The results are compared to analytical solutions, if available, results obtained with standard SPH discretizations, results obtained using the Taylor–Galerkin algorithm with FEM and other results from the literature.

2. Model equations

The mathematical model uses a stress-velocity mixed formulation. The balance of momentum equation is written as:

$$div\,\boldsymbol{\sigma} = \rho\frac{\partial \mathbf{v}}{\partial t}, \tag{1}$$

where $\boldsymbol{\sigma}$ is the stress tensor, ρ the density and $\mathbf{v}$ the velocity vector. For simplicity, body forces have not been included in the analysis. It will be assumed that the material behaviour can be described by Perzyna's viscoplastic law [28]:

$$\frac{\partial \boldsymbol{\sigma}}{\partial t} = \mathbf{D}^e : \left(\frac{\partial \boldsymbol{\varepsilon}}{\partial t} - \frac{\partial \boldsymbol{\varepsilon}^{vp}}{\partial t}\right), \tag{2}$$

where $\mathbf{D}^e$ is the elastic constitutive tensor, $\boldsymbol{\varepsilon}$ the strain tensor and the superindex vp refers to the viscoplastic component of the strain tensor, which is given by:

$$\frac{\partial \boldsymbol{\varepsilon}^{vp}}{\partial t} = \gamma \mathbf{m}\langle\phi(F)\rangle. \tag{3}$$

In above, $\langle\cdot\rangle$ are the Macaulay brackets, the scalar γ is the fluidity parameter, and $\mathbf{m}$ characterizes the direction of the plastic flow. Among the several alternative choices for the function $\phi(F)$, it will be used here

$$\phi(F) = \left(\frac{F - F_0}{F_0}\right)^N, \tag{4}$$

where N is a model parameter and F is a function describing a convex surface in the stress space. The value F_0 characterizes the stress level below which no flow occurs. In the case of a Von Mises material, F is taken as the effective deviatoric stress $\bar{\sigma}$

$$F = \bar{\sigma} = \sqrt{\frac{3}{2}s_{ij}s_{ij}} \tag{5}$$

being $\mathbf{s}$ the deviatoric stress tensor. The size of the yield surface $F_0 = \sigma_0$ will vary according to a suitable hardening/softening law. It will be assumed a linear dependence on the equivalent deviatoric plastic strain $\bar{\varepsilon}^{vp}$

$$\frac{\partial \bar{\sigma}_0}{\partial t} = H\frac{\partial \bar{\varepsilon}^{vp}}{\partial t}, \tag{6}$$

where H is the hardening/softening modulus.

It will be also assumed an associated flow rule

$$\mathbf{m} = \frac{\partial F}{\partial \boldsymbol{\sigma}}. \tag{7}$$

Finally, to express the rate of stress in terms of the gradient of velocity, the kinematic relation is used:

$$\frac{\partial \varepsilon_{ij}}{\partial t} = \frac{1}{2}\left(\frac{\partial v_i}{\partial x_j} + \frac{\partial v_j}{\partial x_i}\right). \tag{8}$$

For convenience, a vector representation of stress, strain and constitutive tensors will be used. In two dimensional situations, stress and strain are represented as

$$\boldsymbol{\sigma} = (\sigma_{11}, \sigma_{22}, \sigma_{12})^T \\ \boldsymbol{\varepsilon} = (\varepsilon_{11}, \varepsilon_{22}, 2\varepsilon_{12})^T \tag{9}$$

Introducing the strain operator $\mathbf{S}$

$$\mathbf{S} = \begin{pmatrix} \partial_x & 0 \\ 0 & \partial_y \\ \partial_y & \partial_x \end{pmatrix}, \tag{10}$$

the balance of momentum and constitutive equations can be written as

$$\frac{\partial \mathbf{v}}{\partial t} = \frac{1}{\rho}\mathbf{S}^T\boldsymbol{\sigma} \tag{11}$$

and

$$\frac{\partial \boldsymbol{\sigma}}{\partial t} = \mathbf{D}^e\mathbf{S}\mathbf{v} - \mathbf{D}^e\frac{\partial \boldsymbol{\varepsilon}^{vp}}{\partial t} \tag{12}$$

Therefore, it is a system of first order hyperbolic equations, where the nonlinearity affects only the source term $\mathbf{D}^e\frac{\partial \boldsymbol{\varepsilon}^{vp}}{\partial t}$.

The momentum and constitutive Eqs. (11) and (12) can be written as

$$\frac{\partial}{\partial t}\begin{bmatrix}\sigma_{11}\\ \sigma_{22}\\ \sigma_{12}\\ v_1\\ v_2\end{bmatrix} - \frac{\partial}{\partial x}\begin{bmatrix}D_{11}v_1\\ D_{12}v_1\\ D_{33}v_2\\ \frac{\sigma_{11}}{\rho}\\ \frac{\sigma_{12}}{\rho}\end{bmatrix} - \frac{\partial}{\partial y}\begin{bmatrix}D_{12}v_2\\ D_{22}v_2\\ D_{33}v_1\\ \frac{\sigma_{12}}{\rho}\\ \frac{\sigma_{22}}{\rho}\end{bmatrix} = \begin{bmatrix}-D_{11}\frac{\partial \varepsilon_{11}^{vp}}{\partial t} - D_{12}\frac{\partial \varepsilon_{22}^{vp}}{\partial t}\\ -D_{12}\frac{\partial \varepsilon_{11}^{vp}}{\partial t} - D_{22}\frac{\partial \varepsilon_{22}^{vp}}{\partial t}\\ -D_{33}\frac{\partial \varepsilon_{12}^{vp}}{\partial t}\\ 0\\ 0\end{bmatrix}, \tag{13}$$

where D_{ij} are the components of the elastic matrix $\mathbf{D}^e$.

Above system can be written alternatively as

$$\frac{\partial \mathbf{U}}{\partial t} + \frac{\partial \mathbf{F}_x}{\partial x} + \frac{\partial \mathbf{F}_y}{\partial y} = \mathbf{S}, \tag{14}$$

where

$$\mathbf{U}^T = (\sigma_{11}\ \ \sigma_{22}\ \ \sigma_{12}\ \ v_1\ \ v_2),$$
$$\mathbf{F}_x^T = (-D_{11}v_1\ \ -D_{12}v_1\ \ -D_{33}v_2\ \ -\frac{\sigma_{11}}{\rho}\ \ -\frac{\sigma_{12}}{\rho}),$$
$$\mathbf{F}_y^T = (-D_{12}v_2\ \ -D_{22}v_2\ \ -D_{33}v_1\ \ -\frac{\sigma_{12}}{\rho}\ \ -\frac{\sigma_{22}}{\rho}),$$
$$\mathbf{S}^T = (-D_{11}\frac{\partial \varepsilon_{11}^{vp}}{\partial t} - D_{12}\frac{\partial \varepsilon_{22}^{vp}}{\partial t}\ \ -D_{12}\frac{\partial \varepsilon_{11}^{vp}}{\partial t} - D_{22}\frac{\partial \varepsilon_{22}^{vp}}{\partial t}\ \ -D_{33}\frac{\partial \varepsilon_{12}^{vp}}{\partial t}\ 0\ 0)$$

or, in a more compact manner

$$\frac{\partial \mathbf{U}}{\partial t} + div\,\mathbf{F} = \mathbf{S} \tag{15}$$

being $\mathbf{U}$ the unknown vector, $\mathbf{F}$ the advective flux tensor and $\mathbf{S}$ the source vector.

3. Numerical discretization

To solve the system of partial differential equations given above, (15), the traditional SPH method applies first the SPH space discretization, obtaining a set of simultaneous ordinary differential equations with respect to time, and this set of equations is then integrated in time using one of the standard techniques such as Euler, leap-frog, predictor–corrector or one of the Runge–Kutta schemes. In most cases, numerical integration of the field variables is carried out at every particle, and thus instabilities due to rank deficiency arise.

In the case of discontinuous functions, such as shock waves, these standard methods present additional numerical problems, like numerical dispersion and diffusion, close to the discontinuities.

To solve the problem of the shock waves propagation, the authors propose in this paper an alternative method which consists of applying first the time discretization by means of a Taylor series expansion in two steps and thereafter the space discretization using a corrected SPH. In the following, the new method presented herein will be referred to as TSPH, which stands for Taylor-SPH.

3.1. Two-steps time discretization

Time discretization of Eq. (15) is carried out by means of a Taylor series expansion in time of $\mathbf{U}$ up to second order accuracy:

$$\mathbf{U}^{n+1} = \mathbf{U}^n + \Delta t\frac{\partial \mathbf{U}}{\partial t}\Big|^n + \frac{\Delta t^2}{2}\frac{\partial^2 \mathbf{U}}{\partial t^2}\Big|^n + O(\Delta t)^3. \tag{16}$$

The first order time derivative of the unknowns can be calculated using Eq. (15)

$$\frac{\partial \mathbf{U}}{\partial t}\Big|^n = (\mathbf{S} - div\,\mathbf{F})^n. \tag{17}$$

The second order derivative with respect to time is given by

$$\frac{\partial^2 \mathbf{U}}{\partial t^2}\Big|^n = \frac{\partial}{\partial t}(\mathbf{S} - div\,\mathbf{F})^n = \left(\frac{\partial \mathbf{S}}{\partial t}\right)^n - div\left(\frac{\partial \mathbf{F}}{\partial t}\right)^n. \tag{18}$$

First step: In order to obtain the time derivatives of fluxes and sources at time t^n, the values of the unknowns at an intermediate time $t^{n+1/2}$ will be obtained first:

$$\mathbf{U}^{n+1/2} = \mathbf{U}^n + \frac{\Delta t}{2}(\mathbf{S} - div\,\mathbf{F})^n. \tag{19}$$

Using the computed value of $\mathbf{U}^{n+1/2}$ it is possible to obtain the fluxes and sources:

$$\left(\frac{\partial \mathbf{F}}{\partial t}\right)^n = \frac{2}{\Delta t}(\mathbf{F}^{n+1/2} - \mathbf{F}^n) \quad \text{and} \quad \left(\frac{\partial \mathbf{S}}{\partial t}\right)^n = \frac{2}{\Delta t}(\mathbf{S}^{n+1/2} - \mathbf{S}^n), \tag{20}$$

which can be substituted in Eq. (18), resulting on

$$\frac{\partial^2 \mathbf{U}}{\partial t^2}\Big|^n = \frac{2}{\Delta t}\left(\mathbf{S}^{n+1/2} - \mathbf{S}^n - div(\mathbf{F}^{n+1/2} - \mathbf{F}^n)\right). \tag{21}$$

Second step: Substituting now the expressions obtained for the first and second order time derivatives, (17) and (21), in the Taylor series expansion (16) we obtain,

$$\mathbf{U}^{n+1} = \mathbf{U}^n + \Delta t(\mathbf{S} - div\,\mathbf{F})^{n+1/2}. \tag{22}$$

3.2. Space discretization: Smoothed Particle Hydrodynamics

3.2.1. Discrete approximation of functions

Space discretization of Eq. (22) is carried out using a corrected SPH. For the sake of completeness, a brief summary of the method is presented herein. For more details about the SPH method and its applications one can be referred to relevant literature [4,5,16,25,27].

In the SPH method each function f is represented by its integral approximation, which is defined by:

$$\langle f(\mathbf{x})\rangle = \int_\Omega f(\mathbf{x}')W(\mathbf{x}' - \mathbf{x}, h)d\mathbf{x}' \tag{23}$$

where the brackets denote a kernel approximation, $\mathbf{x}$ and $\mathbf{x}'$ are the coordinates vectors, $W(\mathbf{x}' - \mathbf{x}, h)$ is the kernel function and h is the

smoothing length that defines the size of the kernel support. The integration is performed in the entire domain Ω. The accuracy of the SPH method depends on the properties of the kernel $W(\mathbf{x}' - \mathbf{x}, h)$: it must be a positive, normalized function and a compact support is required [16].

In most SPH procedures an Eulerian kernel is used, $W(\mathbf{x}'(t) - \mathbf{x}, h(\mathbf{x}, t))$, which is expressed in terms of spatial coordinates. The radius h of the support domain may depend on the spatial coordinates as well. Belytschko et al. [2] have shown that particle discretizations of solids with an Eulerian kernel lead to a distortion of the stable domain of the material in stress space; the tensile instability is one manifestation of this distortion.

On the contrary, the Lagrangian kernel is expressed in terms of material coordinates, $W(\mathbf{X}' - \mathbf{X}, h_0)$, and the neighbours of influence do not change during the course of the simulation. This is a disadvantage in simulating problems with very large distortions. However, it has been shown by Belytschko et al. [2] that the Lagrangian kernel eliminates the tensile instability, and therefore it will be used here since it provides a more consistent procedure.

Several kernels have been proposed in the past and a large number of kernel functions are discussed in literature ranging from polynomial to Gaussian. In this work the B-spline function based on the cubic spline functions introduced by Monaghan and Lattanzio [25] has been used:

$$W(\xi) = C\begin{cases} \left(\frac{2}{3} - \xi^2 + \frac{1}{2}\xi^3\right) & 0 \leqslant \xi \leqslant 1, \\ \frac{1}{6}(2-\xi)^3 & 1 \leqslant \xi \leqslant 2, \\ 0 & \xi \geqslant 2, \end{cases} \tag{24}$$

where $\xi = \frac{|\mathbf{X}' - \mathbf{X}|}{h_0} = \frac{r}{h_0}$; and C is a scaling factor which depends on the dimension of the problem, being

$$C = \begin{cases} \frac{1}{h_0} & \text{for dim} = 1, \\ \frac{15}{7\pi h_0^2} & \text{for dim} = 2, \\ \frac{3}{2\pi h_0^3} & \text{for dim} = 3. \end{cases} \tag{25}$$

The integral approximation of the function (23) is valid at a continuum level, but it is necessary to approximate this integral in a discrete manner, which is called "particle approximation". Then the discrete approximation of expression (23) can be written as:

$$f_I = \sum_{J=1}^{N} f(\mathbf{X}_J) W_{IJ} \frac{m_J}{\rho_J}, \tag{26}$$

where the summation subscript J denotes a particle label and runs over all particles, N, inside the domain, such that $|\mathbf{X}_J - \mathbf{X}_I| \leqslant \kappa h_0$, being κ a positive, constant parameter related to the smoothing function; m_J and ρ_J are the mass and density associated to particle J. The value of the kernel $W(\mathbf{X}_J - \mathbf{X}_I, h_0)$, denoted from now on as W_{IJ}, is the value of the kernel centred at node I at position J.

3.2.2. Discrete approximation of derivatives

The integral representation of the derivative of a scalar function $f(\mathbf{X})$ with SPH is given by

$$\langle \nabla f(\mathbf{X}) \rangle = -\int_{\Omega} f(\mathbf{X}') \nabla W(\mathbf{X}' - \mathbf{X}, h_0) d\mathbf{X}', \tag{27}$$

where ∇W is the derivative of W with respect to $\mathbf{X}'$.

The discrete form is thus obtained using the following expression

$$\nabla f_I = \sum_{J=1}^{N} \frac{m_J}{\rho_J} (f(\mathbf{X}_J) - f(\mathbf{X}_I)) \nabla W_{IJ}, \tag{28}$$

where

$$\nabla f_I = \langle \nabla f(\mathbf{X}_I) \rangle,$$
$$\nabla W_{IJ} = \frac{W'}{h_0} \frac{\mathbf{X}_{IJ}}{r_{IJ}},$$
$$\mathbf{X}_{IJ} = \mathbf{X}_I - \mathbf{X}_J,$$
$$r_{IJ} = |\mathbf{X}_{IJ}|$$

and, for a vectorial function $\mathbf{f}(\mathbf{X})$:

$$\langle div \mathbf{f}(\mathbf{X}_I) \rangle = \nabla \cdot \mathbf{f}_I = \sum_{J=1}^{N} \frac{m_J}{\rho_J} (\mathbf{f}_J - \mathbf{f}_I) \nabla W_{IJ}. \tag{29}$$

3.2.3. Corrected form of the kernel approximation

One of the major drawbacks of the SPH method is the boundary deficiency problem. To overcome this problem, several methods have been proposed in the past [8,14,15,33]. Johnson and Beissel [14] noted that errors in the extensional strains due to lack of linear completeness could be corrected by simple scaling, thus improving accuracy. A correction that enables the derivatives of constant or linear fields to be reproduced exactly was developed by Randles and Libersky [33]. They called that correction normalization (NSPH). Krongauz and Belytschko [15] developed a similar correction and extended those ideas to large deformations.

It is developed here a correction for a Lagrangian kernel based on the normalization proposed by Randles and Libersky [33], which is a straightforward extension of their work.

3.2.3.1. Corrected form of the kernel approximation for a function. The form of the kernel approximation for a function in a multi-dimensional space is the same as the one in one-dimensional space. Performing the Taylor series expansion of function $f(\mathbf{X})$, multiplying by the smoothing function W, integrating over the support domain Ω and neglecting the terms involving derivatives we arrive to the corrective kernel approximation for the function:

$$f_I = \frac{\sum_{J=1}^{N} f(\mathbf{X}_J) W_{IJ} \Omega_J}{\sum_{J=1}^{N} W_{IJ} \Omega_J} = \sum_{J=1}^{N} f(\mathbf{X}_J) \widetilde{W}_{IJ} \Omega_J, \tag{30}$$

where $\Omega_J = \frac{m_J}{\rho_J}$ is the volume associated to particle J and $\widetilde{W}_{IJ}$ is given by:

$$\widetilde{W}_{IJ} = \frac{W_{IJ}}{\sum_{J=1}^{N} W_{IJ} \Omega_J}. \tag{31}$$

It is important to note here that the denominator of above equation is unity for those particles whose support domain does not intersect the boundary.

3.2.3.2. Corrected form of the kernel approximation for the derivatives. To obtain the corrective kernel approximation for the first derivatives of a function it is necessary to perform again the Taylor series expansion of $f(\mathbf{X})$ and neglect the second derivative terms. Multiplying by the first derivatives of the smoothing function, integrating over the support domain Ω and applying the particle approximation we arrive to the corrective kernel approximation for the first derivatives of the function at particle I. However, in a multi-dimensional space the kernel approximation of the three first derivatives is more complicated than in one-dimensional space since the three equations representing the kernel approximations of the derivatives are coupled together:

$$\nabla f_I = \mathbf{C}_I \mathbf{B}_I \tag{32}$$

with

$$\mathbf{C}_I = \left(\sum_{J=1}^{N} \mathbf{X}_{IJ} \otimes \nabla W_{IJ} \Omega_J \right)^{-1} \tag{33}$$

and

$$\mathbf{B}_I = \sum_{J=1}^{N} f_{IJ} \nabla W_{IJ} \Omega_J \tag{34}$$

being $f_{IJ} = f(\mathbf{X}_I) - f(\mathbf{X}_J)$; $\mathbf{X}_{IJ} = \mathbf{X}_I - \mathbf{X}_J$ and $\Omega_J = \frac{m_J}{\rho_J}$.

Eq. (32) can be written alternatively as

$$\nabla f_I = \sum_{J=1}^{N} f_{IJ} \widetilde{\nabla} W_{IJ} \Omega_J, \tag{35}$$

where

$$\widetilde{\nabla} W_{IJ} = \mathbf{C}_I \nabla W_{IJ}. \tag{36}$$

This modification of the SPH approximation for the gradient of a function f, allows the method to fulfil the first-order completeness, enabling the derivatives of constant or linear fields to be reproduced exactly.

3.2.4. Proposed SPH discretization of model equations

Particle methods suffer from tensile instabilities. To stabilize SPH, Dyka and co-workers [10,11] introduced stress points into SPH. This approach was later extended to higher dimensions by Randles and Libersky [32]. It was shown in [2] that the stress point technique stabilizes SPH by suppressing spurious singular modes observed in SPH, but it does not eliminate the distortion of the domain of material instability.

Belytschko et al. [2] pointed out that the tensile instability can be avoided by using a Lagrangian kernel and they showed as well that stress points only remove the instability that arises due to rank deficiency, i.e. spurious singular modes.

As it was explained before, in this work a new SPH formulation is proposed (TSPH). The numerical model is formulated in terms of stress and velocity and a corrected Lagrangian kernel is used for the spatial discretization with SPH. The time discretization is carried out in two steps by means of a Taylor series expansion. This new SPH formulation avoids numerical instabilities and minimizes numerical dispersion and diffusion.

To perform the proposed time discretization, it is necessary the use of an auxiliary set of particles: the "virtual" particles. This auxiliary set of particles will allow the calculation of the unknowns at an intermediate time $t^{n+1/2}$. Otherwise, the time discretization could not be carried out in two steps. These "virtual" particles will be interspersed among the "real" particles in a similar manner it was done in stress-point integration methods. Fig. 1 shows the arrangement of "real" and "virtual" particles in one and two dimensions.

As it was shown in Section 3.1, time discretization of model equations is carried out in two steps:

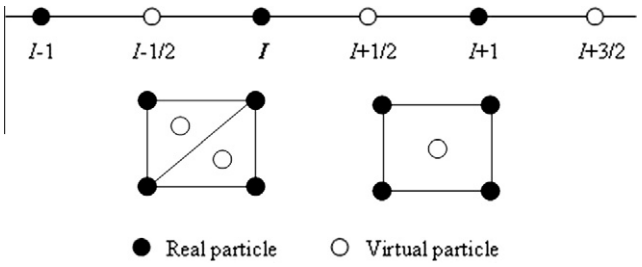

Fig. 1. "Real" and "virtual" particles in one and two dimensions.

- In the first step, the values of the field variables at time $t^{n+1/2}$ are computed by means of Eq. (19) at the positions of the Nv "virtual" particles.
- In the second step, the values of the field variables at time t^{n+1} are computed, using Eq. (22), at the positions of the Nr "real" particles.

First step: Applying SPH spatial discretization to the first step of time discretization, (19), we obtain:

$$\langle \mathbf{U} \rangle_{VP}^{n+1/2} = \langle \mathbf{U} \rangle_{VP}^{n} + \left\langle \frac{\Delta t}{2} \right\rangle \left[\langle \mathbf{S} \rangle_{VP}^{n} - \langle div\, \mathbf{F} \rangle_{VP}^{n} \right], \tag{37}$$

where the subscript VP indicates that the values of $\mathbf{U}$, $\mathbf{S}$ and $div\,\mathbf{F}$ are computed at the positions of the "virtual" particles.

Using the corrected form for the approximation of functions and derivatives given by Eqs. (30) and (35), the value of the variable $\mathbf{U}$ at $t^{n+1/2}$ is obtained:

$$\mathbf{U}_{VP}^{n+1/2} = \mathbf{U}_{VP}^{n} + \frac{\Delta t}{2} \left[\sum_{J=1}^{Nr} \frac{m_J}{\rho_J} \mathbf{S}_J^n \widetilde{W}_{IJ} - \sum_{J=1}^{Nr} \frac{m_J}{\rho_J} \mathbf{F}_J^n \widetilde{\nabla} W_{IJ} \right] \tag{38}$$

being J the "real" particles, such that $|\mathbf{X}_J - \mathbf{X}_{VP}| \leqslant 2h_0$.

Second step: Applying SPH spatial discretization to Eq. (22), we obtain

$$\langle \mathbf{U} \rangle_{RP}^{n+1} = \langle \mathbf{U} \rangle_{RP}^{n} + \langle \Delta t \rangle \left[\langle \mathbf{S} \rangle_{RP}^{n+1/2} - \langle div\, \mathbf{F} \rangle_{RP}^{n+1/2} \right], \tag{39}$$

where the subscript RP indicates that the values of $\mathbf{U}$, $\mathbf{S}$ and $div\,\mathbf{F}$ are computed at the positions of the "real" particles.

Using expressions (30) and (35), the value of the variable $\mathbf{U}$ at t^{n+1} is obtained:

$$\mathbf{U}_{RP}^{n+1} = \mathbf{U}_{RP}^{n} + \Delta t \left[\sum_{J=1}^{Nv} \frac{m_J}{\rho_J} \mathbf{S}_J^{n+1/2} \widetilde{W}_{IJ} - \sum_{J=1}^{Nv} \frac{m_J}{\rho_J} \mathbf{F}_J^{n+1/2} \widetilde{\nabla} W_{IJ} \right], \tag{40}$$

where J are the "virtual" particles, such that $|\mathbf{X}_J - \mathbf{X}_{RP}| \leqslant 2h_0$.

The particle masses and volumes needed to calculate (38) and (40) are obtained via Voronoi tessellation. In the 2D procedure, a structured quadrilateral particle arrangement is used. As it is shown in Fig. 2: 4 "real" particles are arranged so they form a square and a "virtual" particle for the calculations at $t^{n+1/2}$ is placed in the centroid of the square. In this particular case, computation of particles volumes is especially easy. The square is then subdivided into 4 more squares for computation of the volumes, and once the

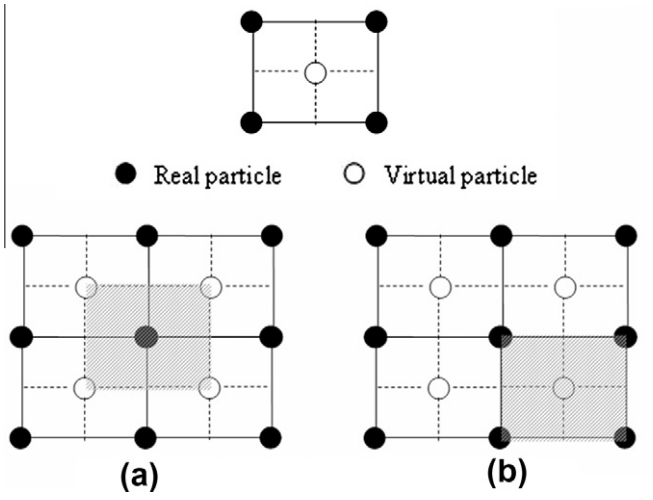

Fig. 2. "Real" and "virtual" particles arrangement in a structured quadrilateral configuration: (a) quadrilateral volume of "real" particles; (b) quadrilateral volume of "virtual" particles.

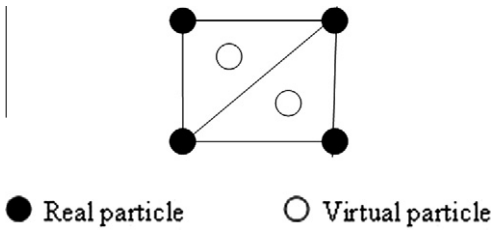

Fig. 3. "Real" and "virtual" particles arrangement in a triangular configuration.

coordinates of the "real" and "virtual" particles are known, quadrilateral volumes can easily be computed as it is shown in Fig. 2. It is important to note here that in the first step, (38), only volumes of "real" particles are considered, while in the second step, (40), only volumes of "virtual" particles are taken into account. As a consequence of that, at time t^n the total initial volume coincides with the sum of the "real" particles volumes, while at $t^{n+1/2}$ the total initial volume will be the sum of the "virtual" particles volumes. It is also important to mention that particle masses and volumes have to be calculated only once at the beginning of the computation as long as the kernels are Lagrangian.

Identical procedure would be applied if a structured triangular configuration was adopted (see Fig. 3). But in this case computation of volumes is not as straight as in the structured quadrilateral configuration, and a Voronoi diagram would be needed. This is also the case when using an unstructured arrangement of particles. Nevertheless it can be shown that the proposed algorithm does not depend on the particles configuration provided the difference in distance among them does not become too large.

Traditional SPH formulations are written in terms of displacements, and therefore essential boundary conditions for displacements and natural boundary conditions for tractions must be taken into account. On the contrary, in the method proposed herein the model equations are formulated in terms of stress and velocity, and thus only essential boundary conditions must be considered. The boundary particles are located exactly on the boundary lines of the domain and the essential boundary conditions are enforced directly at each particle on the boundary lines where the variables are prescribed.

4. Numerical examples

Numerical modelling of the propagation of waves that present discontinuities, such as shock waves, presents some major difficulties: numerical dispersion and diffusion problems. The amplitude of the wave decreases due to numerical damping and oscillations appear at the discontinuities of the wave due to the numerical dispersion of the scheme.

The purpose of this section is to present some examples which will show the performance of the proposed algorithm in both elastic and viscoplastic problems.

The three examples which will be considered next have been chosen in order to illustrate:

(i) Reasonable numerical damping and dispersion properties. In the case of shock waves, trailing oscillations and damping are minimized.
(ii) Good performance in bending dominated situations using a small number of particles.
(iii) When applied to localization problems, the proposed algorithm performs well in capturing the shear band.
(iv) The proposed method eliminates numerical instabilities inherent to traditional SPH formulations.

4.1. Propagation of a shock wave on a 1D bar

In this section, the problem of a shock wave propagating in both, an elastic and viscoplastic bars, using the proposed TSPH method will be solved. It will be shown that the results obtained with this method are: (i) more accurate than those obtained using a similar time discretization with FEM (Taylor–Galerkin); (ii) more accurate that those obtained using a standard time discretization with SPH.

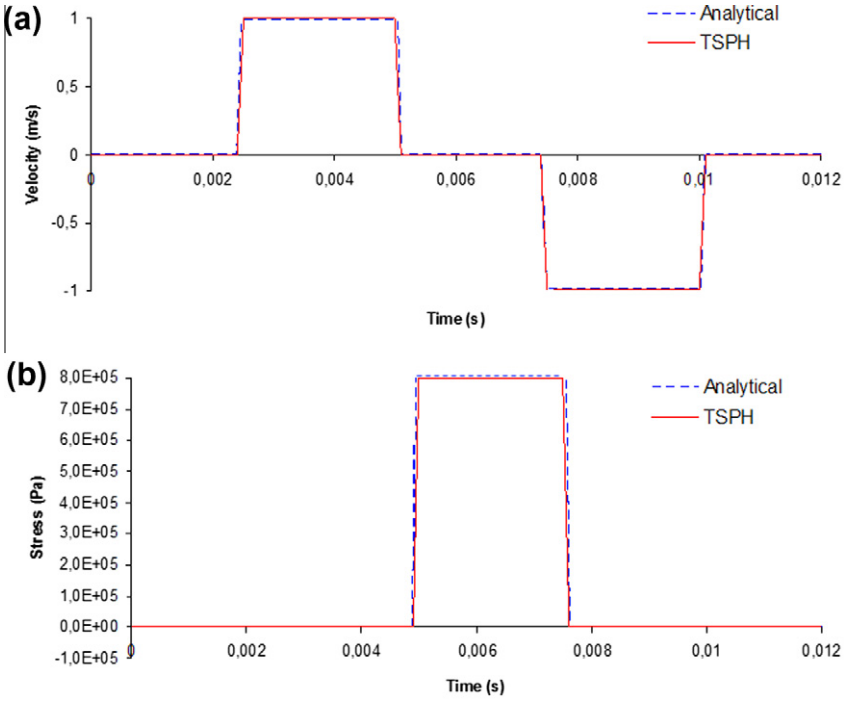

Fig. 4. Elastic case using TSPH: (a) velocity at 0.5 m as a function of time and (b) stress at the fixed end ($L = 1$ m) as a function of time.

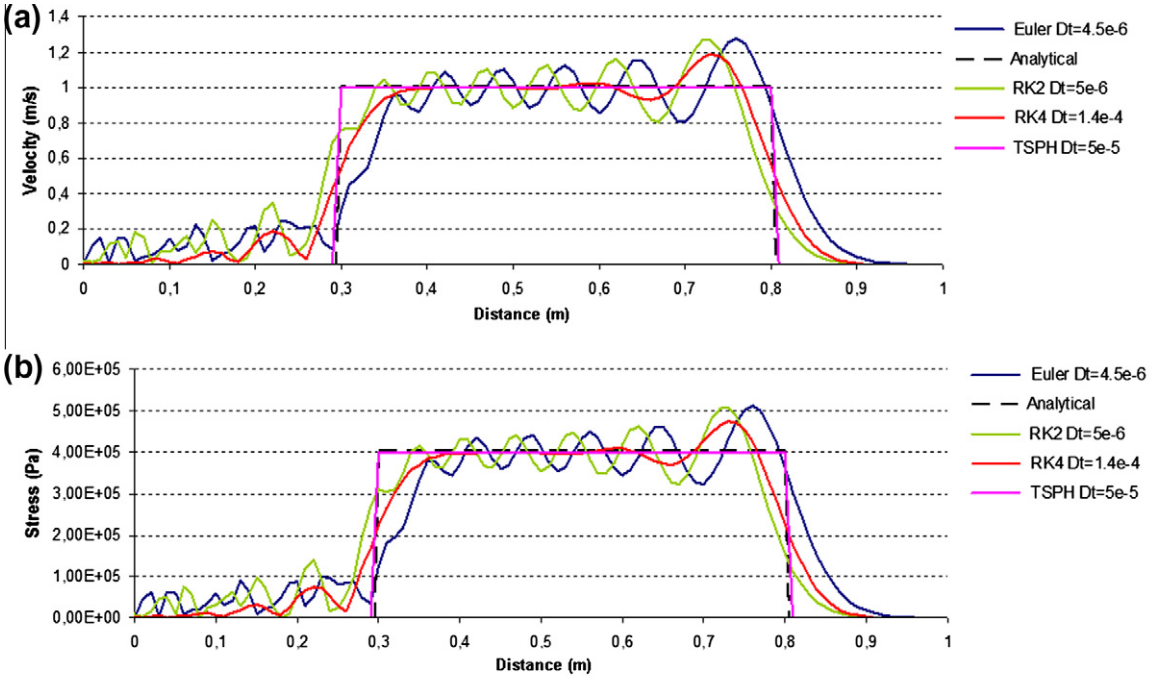

Fig. 5. Comparison among TSPH and standard time discretizations with SPH (Euler, second order Runge–Kutta and fourth order Runge–Kutta), and time-steps used in the analyses (Dt): (a) velocity and (b) stress, along the bar for $t = 4 \times 10^{-3}$ s in the elastic case.

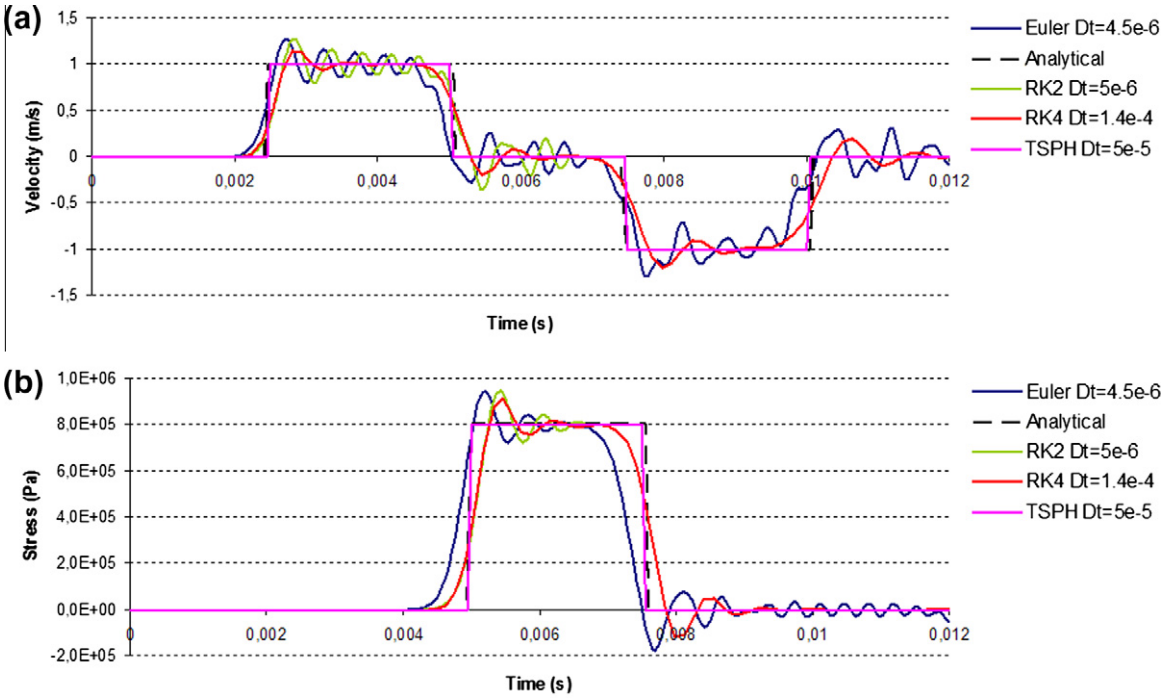

Fig. 6. Comparison among TSPH and standard time discretizations with SPH (Euler, second order Runge–Kutta and fourth order Runge–Kutta), and time-steps used in the analyses (Dt): (a) velocity at 0.5 m and (b) stress at the fixed end ($L = 1$ m), as functions of time in the elastic case.

4.1.1. Elastic case

The problem consists of a bar of length $L = 1$ m with a unit section, which has been spatially discretized using 50 "real" particles and 49 "virtual" particles.

The bar is initially at rest, so that the initial conditions are: $v = 0$; $\sigma = 0$

The applied boundary conditions are the following:

(i) On the left boundary:

$$v(t) = \begin{cases} 1 \text{ m/s} & \text{for } t \leqslant t_f, \\ 0 & \text{for } t > t_f, \end{cases}$$

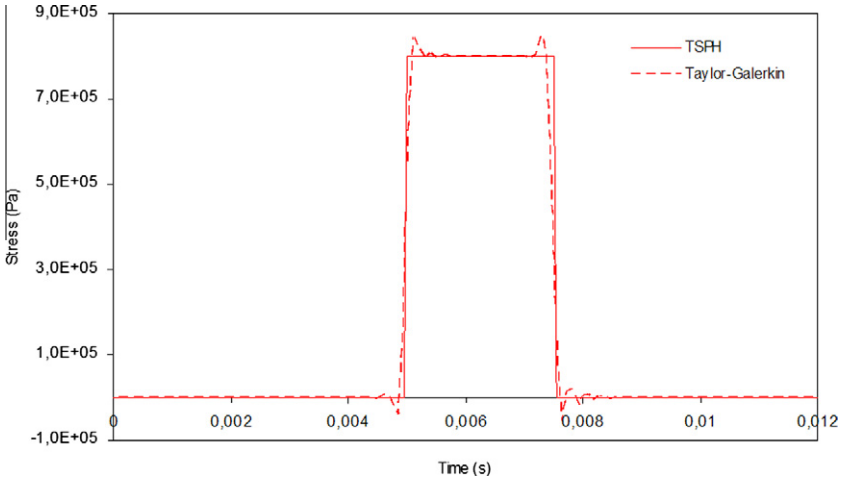

Fig. 7. Stress at the fixed end ($L = 1$ m) as a function of time in the elastic case: TSPH vs Taylor–Galerkin.

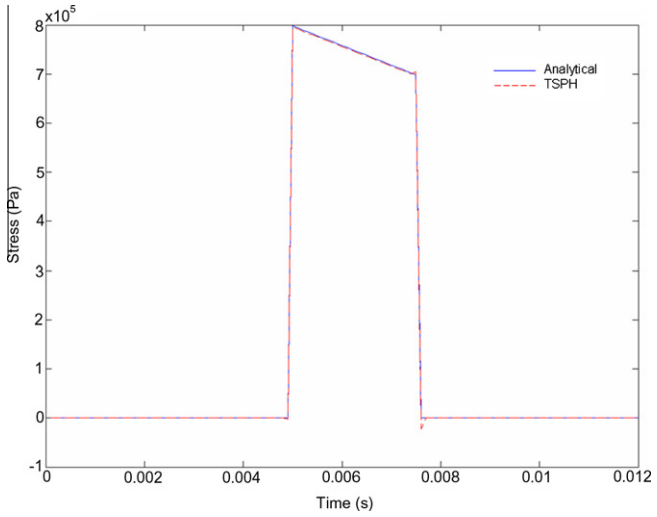

Fig. 8. Stress at the fixed end ($L = 1$ m) in the viscoplastic case for a constant source term ($N = 0$ and $\gamma = 1$). Comparison between analytical and numerical solution with TSPH.

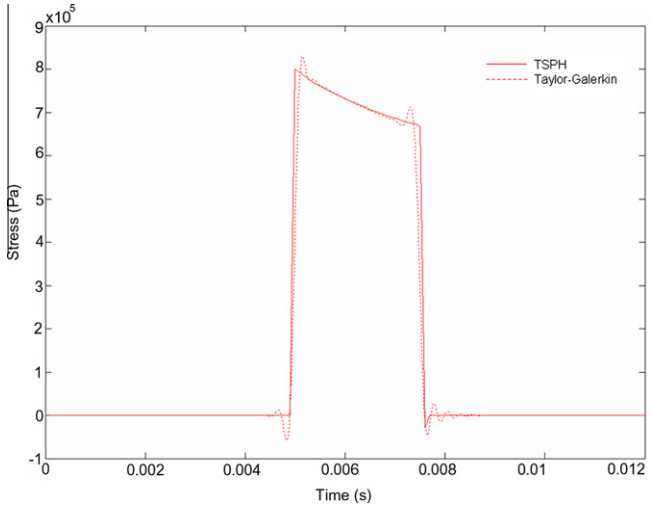

Fig. 9. Stress at the fixed end ($L = 1$ m) in the viscoplastic case ($N = 2$ and $\gamma = 2$): TSPH vs Taylor–Galerkin.

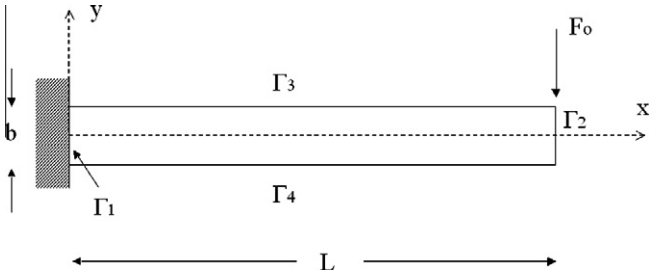

Fig. 10. Sketch of a cantilever beam.

where t_f has been taken as 2.5×10^{-3} s.

(ii) The right boundary is a fixed end, and therefore: $v = 0$.

The material properties are the following: density $\rho = 2000$ kg/m^3 and elastic modulus $E = 8 \times 10^7$ Pa.

There is an analytical solution available for this problem: the incoming wave will propagate towards the right boundary without any distortion and keeping its initial amplitude of $\sigma_0 = v_0\sqrt{\rho E} = 4 \times 10^5$ Pa and $v_0 = 1$ m/s. It will reflect at the fixed end ($L = 1$ m) and the amplitude of σ at this point will be doubled to a value of 8×10^5 Pa, while the velocity of the wave after reflexion will propagate along the bar with $v_0 = -1$ m/s.

Fig. 4 depicts the velocity at 0.5 m and the stress at the fixed end ($L = 1$ m) as functions of time using the TSPH method. The time-step used in the calculation is $\Delta t = 9.9 \times 10^{-5}$ s. It can be observed that no oscillations appear in the front of the wave and the results are in complete agreement with the analytical solution.

In order to show the better performance of the TSPH in comparison with other time discretizations it will be analyzed the problem of the propagation of a shock wave in an elastic bar using the corrected SPH with a Lagrangian kernel when only the time discretization scheme is changed. As it was explained above, traditional SPH methods apply first the SPH space discretization to the partial differential equations and this set of equations is then integrated in time using one of the standard techniques. In this case, the Euler, second order Runge–Kutta (RK2) and fourth order Runge–Kutta (RK4) schemes will be considered for the comparison with TSPH.

Fig. 11. "Real" particles arrangement for a cantilever beam (21 × 3 "real" particles).

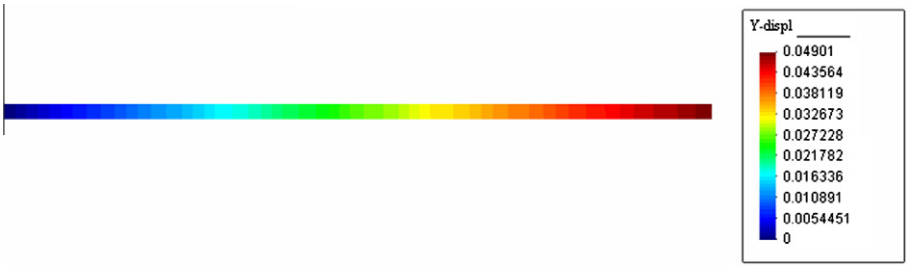

Fig. 12. Bending of a cantilever beam: vertical displacements using the TSPH method.

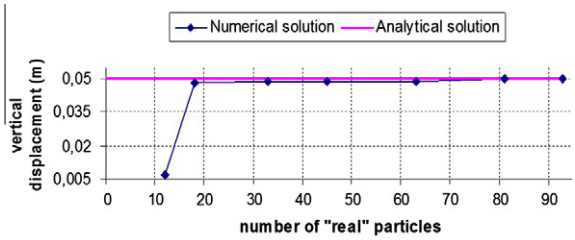

Fig. 13. Convergence analysis for TSPH: variation of deflexion at L = 1 m with an increasing number of "real" particles.

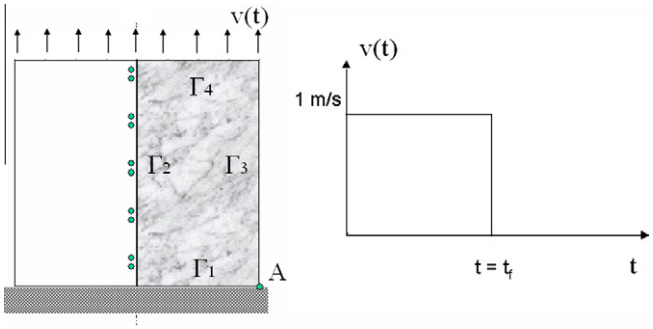

Fig. 14. Sketch of the specimen.

The problem consists again of a bar of length $L = 1$ m with a unit section, which has been spatially discretized using 100 particles (100 "real" particles for TSPH). The problem has been analyzed under the same initial and boundary conditions as in the former case.

Figs. 5 and 6 depict the results obtained for the time discretizations considered for the comparison and the time-steps used in the analyses (Dt). It can be observed that when using a standard time discretization with a corrected SPH numerical oscillations and diffusion are present (even in the case of the fourth order Runge–Kutta scheme, RK4). However, the numerical solution using TSPH is free of oscillations and diffusion and the result is in complete agreement with the analytical solution. It is also worth mentioning that the computational time required for TSPH is about one half the time required for RK4. In addition to that, it was shown in the former example that using TSPH it is possible to reduce the number of particles to one-half (50 "real" particles) and the numerical solution preserves its accuracy.

These results show the good performance and efficiency of the TSPH method in comparison with standard SPH discretizations when solving hyperbolic partial differential equations when discontinuities are present.

The authors of the present paper have published in previous works some different alternatives to solve the propagation of shock waves in solids using FEM [21–23]. In Solid Dynamics, the classical approach of numerical analysis is based on displacement formulation. The shortcomings of this approach can be classified in: (a) numerical damping and numerical dispersion; (b) low-order elements cannot be used as they are not accurate and the results depend on mesh alignment and mesh size. To solve the problems mentioned above the authors have proposed in previous works a numerical model formulated in terms of stress and velocity based on the Taylor–Galerkin scheme.

Fig. 7 depicts a comparison between the results obtained with the proposed TSPH and with Taylor–Galerkin for the stress at the fixed end of the bar after reflection. It can be observed that the TSPH method provides better accuracy than Taylor–Galerkin. In addition to that, the time-step required to get good accuracy with FEM using Taylor–Galerkin ($\Delta t = 9 \times 10^{-6}$ s) is smaller than the time-step required by TSPH ($\Delta t = 5 \times 10^{-5}$ s), and therefore the efficiency of the proposed scheme is higher.

4.1.2. Viscoplastic case

It will be analyzed now the propagation of a shock wave in a viscoplastic softening bar. The Perzyna's viscoplastic model is used here [28].

The problem consists of a bar of length $L = 1$ m with a unit section, which has been spatially discretized using 50 "real" particles and 49 "virtual" particles. The problem has been analyzed under the same initial and boundary conditions as in the elastic case.

To show the performance of the method, the non-linear system of Eq. (15) with a constant source term will be considered (model parameter $N = 0$). There is an analytical solution available in this case, when the shock wave reaches the right end of the bar and reflection occurs. The analytical solution for the stress at the right boundary is given by:

$$\sigma(L,t) = \left[2v_o\sqrt{\rho E} - \frac{1}{2}E\gamma(t-t_o)\right]H\left(\frac{t-t_o}{t_r-t}\right),$$

where $t_o = L\sqrt{\rho/E}$; $t_r = t_o + t_f$ being t_f=2.5 $\times 10^{-3}$ s; $H(t)$ is the Heaviside function:

$$H\left(\frac{t-t_0}{t_r-t}\right) = \begin{cases} 0 & \text{for} \quad t < t_0, \\ 1 & \text{for} \quad t_0 < t < t_r, \\ 0 & \text{for} \quad t > t_r. \end{cases}$$

The material properties have been chosen as follows: density $\rho = 2000\ \text{kg/m}^3$, elastic modulus $E = 8 \times 10^7$ Pa, yield stress $\bar{\sigma}_0 = 4 \times 10^5$ Pa and softening modulus $H = -E/10$. The Perzyna parameters are $N = 0$ and $\gamma = 1\ \text{s}^{-1}$.

Fig. 8 depicts the stress at the fixed end of the bar after reflection has happened. The amplitude of the wave has been chosen such that the stress does not reach the yield stress until the wave is reflected at the fixed end, which happens at $t_0 = 5 \times 10^{-3}$ s. Hereafter, the stress doubles, reaching the yield stress, $\bar{\sigma}$, and the

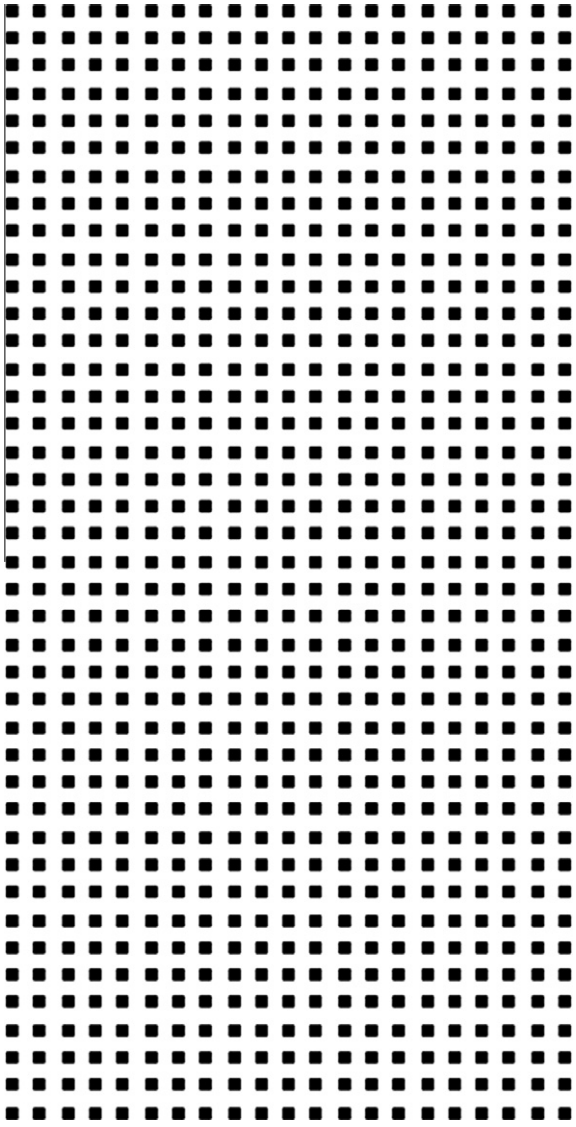

Fig. 15. "Real" particles arrangement (21 × 41 "real" particles).

viscoplastic strain localizes at the right end of the bar. As a result of that the amplitude of the wave is reduced as a function of time. This figure presents the comparison between the analytical solution at $L = 1$ m and the result obtained using the proposed TSPH method. It can be observed that the analytical and the numerical solutions are in complete agreement, and the numerical solution is free of oscillations and diffusion.

The former analysis can be extended for the case of $N \neq 0$, when there is not an analytical solution available. In order to show that the performance of the method does not depend on the source term, the case in which the Perzyna parameters are $N = 2$ and $\gamma = 2\ s^{-1}$ will be considered.

Fig. 9 depicts a comparison between the results obtained with the proposed TSPH and with Taylor–Galerkin for the stress at the fixed end of the bar after reflection (with $N = 2$ and $\gamma = 2\ s^{-1}$). It can be observed that again the TSPH method provides much better accuracy for the propagation of shock waves than Taylor–Galerkin.

Finally, it is worth mentioning that the time-step required to get good accuracy with FEM using Taylor–Galerkin ($\Delta t = 8 \times 10^{-6}$ s) is again smaller than the time-step required by TSPH ($\Delta t = 10^{-4}$ s), and the efficiency of the proposed scheme in this case is also higher.

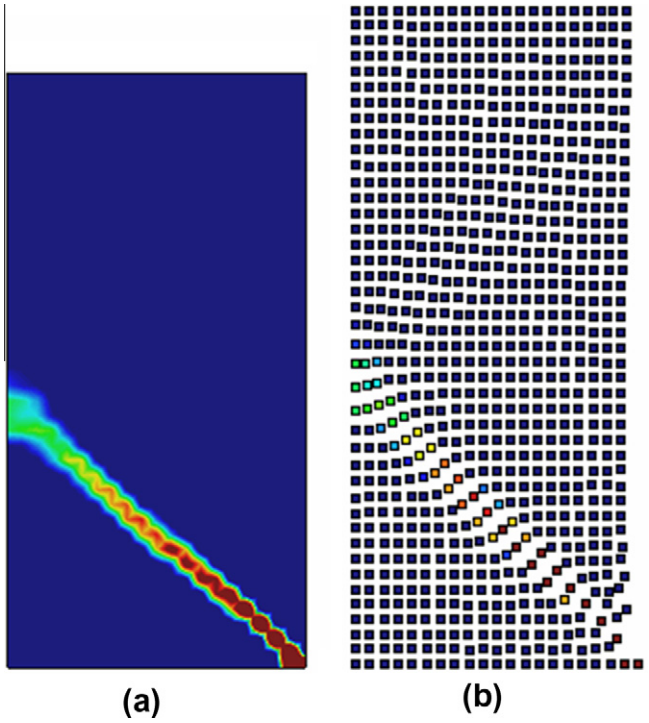

Fig. 16. (a) Viscoplastic strain and (b) deformed configuration (amplification factor = 6) using TSPH (21 × 41 "real" particles).

4.2. Bending of a cantilever beam

The purpose of this example is to show the behaviour of the proposed model in bending dominated situations. With this purpose, it has been chosen the simple example of a cantilever beam subjected to a very slowly increasing vertical load at its free end. The load is kept constant when a certain value F_0 is reached, after which the numerical value obtained for the tip deflection will be compared against its analytical value.

Fig. 10 shows the proposed example. Length and width of the beam are $L = 1$ m and $b = 0.02$ m. Material is assumed to be elastic, with Young's modulus $E = 8 \times 10^9$ Pa and Poisson's ratio $\nu = 0.0$. Density has been taken as 2×10^3 kg/m^3.

A structured arrangement of 63 "real" particles and 40 "virtual" particles is used as it is shown in Fig. 11. As it was explained in Section 3.2.4., every 4 "real" particles form a square with a "virtual" particle placed in its centroid.

Boundary conditions are the following:

(i) Prescribed velocities along Γ_1: $v_x = v_y = 0$.
(ii) Along Γ_3 and Γ_4 it has been assumed $\sigma_{yy} = 0$.
(iii) Along Γ_2 it has been assumed a stress distribution given by

$$\sigma_{xy} = \frac{F_0}{b}\frac{t}{t_0} \quad t < t_0,$$
$$\sigma_{xy} = \frac{F_0}{b} \quad t \geqslant t_0,$$

which corresponds to a load increasing linearly with time until time $t_0 = 5 \times 10^{-5}$ s and then remaining constant as $F_0 = 8 \times 10^2$ N.

The analytical solution of this problem is given by the following expression:

$$y_{\max} = \frac{4L^3}{Eb^2}\sigma_{xy},$$

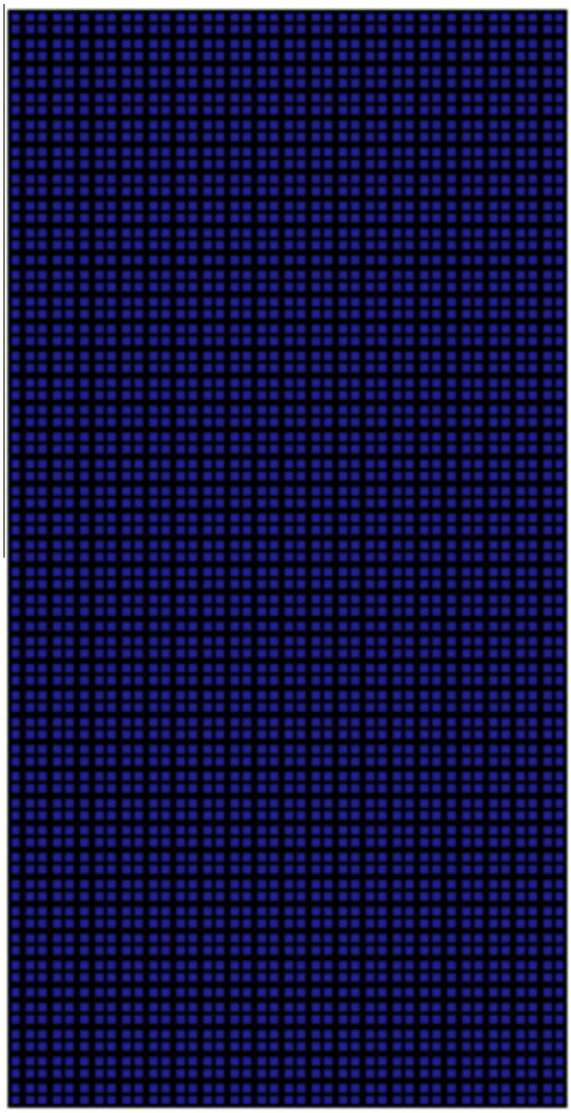

Fig. 17. "Real" particles arrangement (41 × 81 "real" particles).

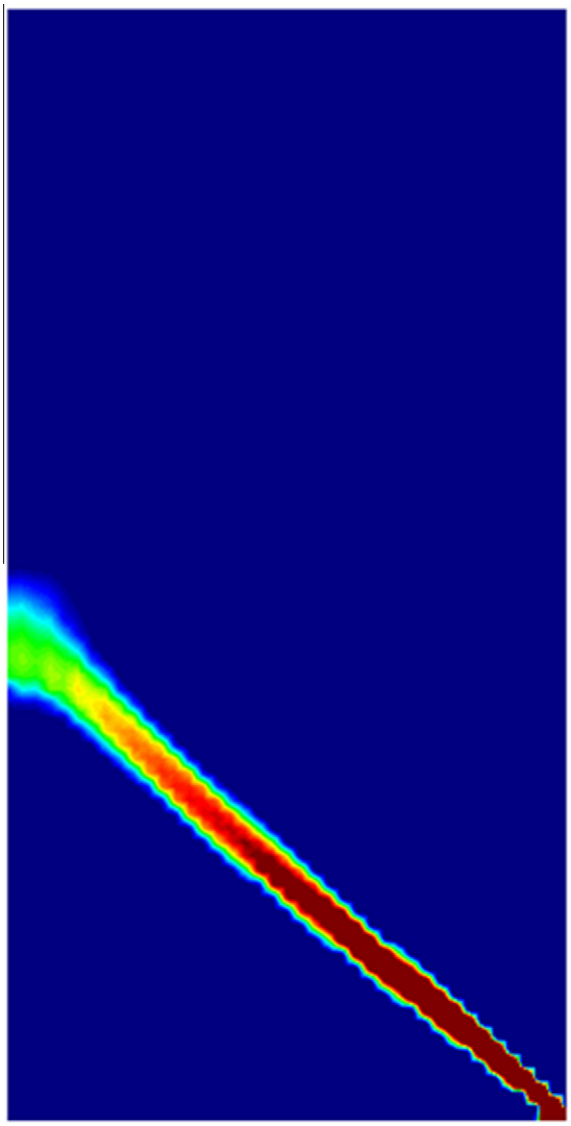

Fig. 18. Viscoplastic strain (41 × 81 "real" particles) using TSPH.

where σ_{xy} is the averaged shear tension applied on the section at the free end of the beam. To get this analytical solution some assumptions have been made: (i) the beam length, L, is much larger than the dimensions of the transversal section, (ii) the beam section does not change when bending occurs, and (iii) small deformations are considered. Taking into account that $L = 1$ m, $b = 0.02$ m, $E = 8 \times 10^9$ Pa and $\sigma_{xy} = 4 \times 10^4$ Pa, the expected maximum vertical displacement for the beam is $y_{\max} = 5 \times 10^{-2}$ m.

Fig. 12 depicts the vertical displacement of the beam obtained with the TSPH method. The time-step used for the calculation is $\Delta t = 2 \times 10^{-9}$ s. The computed numerical value of the maximum deflection obtained at the right end is $y_{\max} = 4.9 \times 10^{-2}$ m, which is in very good agreement with the analytical solution. As it can be observed, the result obtained with the proposed algorithm reaches an acceptable accuracy with a small number of degrees of freedom (63 "real" particles) as well as it seems to be free of instabilities.

In order to study the improvement in the numerical solution for an increasing number of particles a convergence analysis has been accomplished. Fig. 13 depicts the vertical displacement at the right end of the beam as a function of the increasing number of particles.

In this analysis it is shown that the TSPH method converges quickly to the analytical solution and only a small number of particles is required to obtain very accurate results.

So far, it has been proved that the proposed algorithm provides:

(i) Good resolution of shock waves and discontinuities with very low numerical diffusion and dispersion.
(ii) Good accuracy in bending dominated situations.

It will be shown next its performance in capturing shear bands produced in fast dynamics and shock wave propagation problems.

4.3. Strain localization in 2D

It will be analyzed here the case of a two dimensional specimen under plane stress conditions subjected to a shock on its upper face. The specimen has been sketched in Fig. 14 and it consists of a square of side 1 m, but for symmetry reasons only one half will be considered in the analysis.

The domain is discretized using a structured particle arrangement of 861 "real" particles and 800 "virtual" particles (see Fig. 15), so that every 4 "real" particles form a square with a "virtual" particle placed in its centroid.

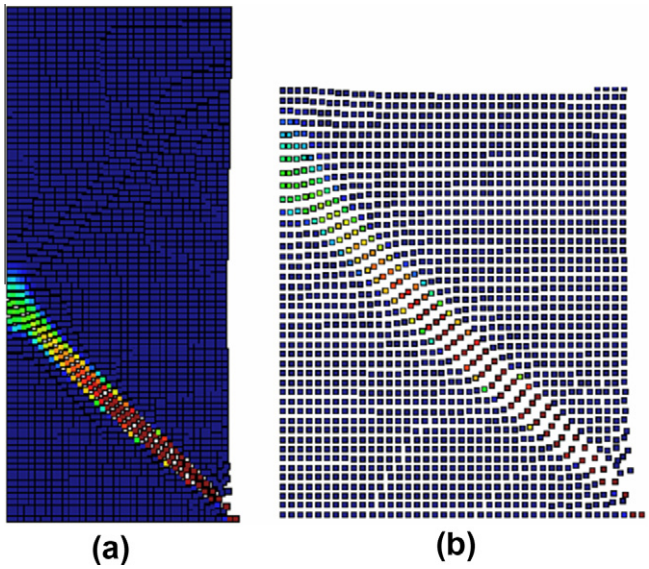

Fig. 19. (a) Deformed configuration (41×81 "real" particles); (b) detail of the deformed configuration in the area close to the shear band (amplification factor = 6).

The applied boundary conditions are the following:

(i) On Γ_1 velocity has been set equal zero: $v_x = v_y = 0$.
(ii) On Γ_2 the symmetry results on $v_x = 0$ and $\sigma_{xy} = 0$.
(iii) Γ_3 is a stress free boundary, and therefore $\sigma_{xx} = 0$ and $\sigma_{xy} = 0$.
(iv) Finally, velocity at Γ_4 is:

$$v_y = v(t),$$

where $v(t)$ is given by:

$$v(t) = \begin{cases} 1 \text{ m/s} & t \leqslant t_f, \\ 0 & t > t_f, \end{cases}$$

where t_f has been taken as 8×10^{-3} s.

The material has been assumed to be viscoplastic, with a yield surface of Von Mises type. The Young's modulus has been taken as $E = 8 \times 10^7$ Pa, Poisson's ratio is $\nu = 0.3$, the initial yield stress is $\sigma = 5 \times 10^5$ Pa and a softening modulus of $H = -E/10$ has been chosen. Parameters of Perzyna's model are $\gamma = 25\ \text{s}^{-1}$ and $N = 1$. Density is $\rho = 2000\ \text{kg/m}^3$.

The wave speed can be computed as follows:

$$c = \sqrt{\frac{E}{\rho}\frac{1-\nu}{(1-2\nu)(1+\nu)}} \approx 232 \text{ m/s}.$$

Fig. 16(a) shows the contours of viscoplastic strain. The time-step used for the calculation is $\Delta t = 9.5 \times 10^{-6}$ s. The amplitude of the wave has been chosen such that the stresses do not reach the yield surface until the wave is reflected at the bottom, which happens at $t = 4.3 \times 10^{-3}$ s. Hereafter, the stress doubles, the stress path crosses the yield surface, and the strain localizes in the form of a shear band which is incepted at point A (see Fig. 14). Inclination of the shear band is close to 45°. It is important to remark that it has not been included any additional disturbance to trigger the shear band, such as a small horizontal load or imperfection. In Fig. 16(b) the deformed configuration of the "real" particles arrangement is depicted with an amplification factor equal to 6.

Finally, the same problem is solved using a structured particle arrangement of 3321 "real" particles and 3200 "virtual" particles (see Fig. 17), to assess whether the results are dependent on the distance among particles. The time-step used for the calculation is $\Delta t = 8 \times 10^{-6}$ s. The contours of plastic strain and the deformed configuration are given in Figs. 18 and 19 (amplification factor = 6). It can be noticed that neither the direction of the shear band nor its width depend on the number of particles used for the calculation.

The main advantage of the proposed method is the small number of particles required to obtain accurate results. As it has been shown, the method is able to capture the shear band using only 861 particles and the result does not differ significantly from that obtained using 3321 particles. The number of particles demanded by other SPH formulations is about 100 times the number of particles required by TSPH and therefore the computational effort is much higher.

5. Conclusions

A two-steps time integration scheme using a corrected SPH has been presented to solve the problem of a shock wave propagating in viscoplastic continua. Equations have been written in terms of stress and velocity, and a Lagrangian kernel has been used for the approximation. Discretization in time has been carried out in two steps using the Taylor series expansion. Two different sets of particles have been used for the computations at each of these two time steps.

The method proposed here has been proved (i) to be able to solve the problem of instabilities inherent to standard discretization techniques used traditionally with SPH; (ii) it is able to capture the shock wave discontinuity avoiding numerical dispersion and diffusion; (iii) it requires only a small number of particles to get accurate results; (iv) it is easy to implement; (v) it is shown to be robust and efficient.

In the first example it has been shown the performance of the proposed method in one-dimensional case, for a shock wave propagating in both elastic and viscoplastic bars. It has been demonstrated how the proposed method provides more accurate solutions than those obtained with a similar time discretization with FEM (Taylor–Galerkin) and than those obtained using a standard time discretization with SPH. In both cases, elastic and viscoplastic, the numerical solution obtained using TSPH is able to capture the shock wave discontinuity avoiding numerical dispersion and diffusion.

In the second numerical example it has been shown the good performance of the method in bending dominated situations. The proposed algorithm exhibits good accuracy and it is able to reproduce the analytical results for bending of a cantilever beam with a small number of particles. It has been shown the fast convergence of the method and the small number of particles required to obtain very accurate results.

Finally, to asses the performance of the method in capturing shear bands, a two-dimensional specimen under plane stress conditions subjected to a shock on its upper face has been considered. It has been shown how the proposed algorithm performs well in capturing the shear band. Numerical instabilities are not present when using this new SPH formulation. The method is shown to be stable, robust and only a reduced number of particles is required to obtain reasonably accurate results.

Acknowledgement

The authors would like to express their gratitude to the Agencia Española de Cooperación Internacional for the economic support granted.

References

[1] S.N. Atluri, S. Shen, The Meshless Local Petrov–Galerkin (MLPG) Method, Tech Science Press, 2002.
[2] T. Belytschko, Y. Guo, W.K. Liu, S.P. Xiao, A unified stability analysis of meshless particle methods, Int. J. Numer. Methods Engrg. 48 (2000) 1359–1400.
[3] T. Belytschko, Y.Y. Lu, L. Gu, Element free Galerkin methods, Int. J. Numer. Methods Engrg. 37 (2) (1994) 229–256.
[4] T. Belytschko, Y. Krongauz, D. Organ, M. Fleming, P. Krysl, Meshless methods: an overview and recent developments, Comput. Methods Appl. Mech. Engrg. 139 (1996) 3–47.
[5] W. Benz, Smooth particle hydrodynamics: a review, in: J.R. Buchler (Ed.), The Numerical Modelling of Nonlinear Stellar Pulsations, Kluwer Academic Publishers, 1990, pp. 269–288.
[6] J. Bonet, S. Kulasegaram, Correction and stabilization of smooth particle hydrodynamics methods with applications in metal forming simulations, Int. J. Numer. Methods Engrg. 47 (2000) 1189–1214.
[7] J. Bonet, T. Lok, Variational and momentum preservation aspects of smooth particle hydrodynamic formulations, Comput. Methods Appl. Mech. Engrg. 180 (1–2) (1999) 97–115.
[8] P.M. Campbell, Some new algorithms for boundary value problems in smooth particle hydrodynamics, Technical Report DNA-TR-88-286, Mission Research Corporation, 1989.
[9] J. Chessa, T. Belytschko, Arbitrary discontinuities in space-time finite elements by level sets and X-FEM, Int. J. Numer. Methods Engrg. 61 (15) (2004) 2595–2614.
[10] C.T. Dyka, R.P. Ingel, An approach for tension instability in smoothed particle hydrodynamics, Comput. Struct. 57 (1995) 573–580.
[11] C.T. Dyka, P.W. Randles, R.P. Ingel, Stress points for tension instability in SPH, Int. J. Numer. Methods Engrg. 40 (1997) 2325–2341.
[12] R.A. Gingold, J.J. Monaghan, Smoothed particles hydrodynamics: theory and application to non-spherical stars, Mon. Not. R. Astron. Soc. 181 (1977) 375–389.
[13] M.I. Herreros, M. Mabssout, M. Pastor, Application of level-set approach to moving interfaces and free surface problems in flow through porous media, J. Comput. Methods Appl. Mech. Engrg. 195 (2006) 1–25.
[14] G.R. Johnson, S.R. Beissel, Normalized smoothing functions for SPH impact computations, Int. J. Numer. Methods Engrg. 39 (1996) 2725–2741.
[15] Y. Krongauz, T. Belytschko, Consistent pseudo derivatives in meshless methods, Comput. Methods Appl. Mech. Engrg. 146 (1997) 371–386.
[16] G.R. Liu, M.B. Liu, Smoothed Particle Hydrodynamics: A Meshfree Particle Method, World Scientific, 2003.
[17] W.K. Liu, S. Jun, Y.F. Zhang, Reproducing kernel particle methods, Int. J. Numer. Methods Fluids 20 (8–9) (2005) 1081–1106.
[18] L.D. Libersky, A.G. Petschek, Smooth Particle Hydrodynamics with Strength of Materials, Advances in the Free Lagrange Method, Lecture Notes in Physics, vol. 395, Springer, Berlin, Heidelberg, 1990, pp. 248–257.
[19] L.D. Libersky, A.G. Petschek, A.G. Carney, T.C. Hipp, J.R. Allahdadi, F.A. High, Strain Lagrangian hydrodynamics: a three-dimensional SPH code for dynamic material response, J. Comput. Phys. 109 (1993) 67–75.
[20] L.B. Lucy, A numerical approach to the testing of fusion process, Astron. J. 82 (1977) 1013–1024.
[21] M. Mabssout, M. Pastor, A Taylor–Galerkin algorithm for shock wave propagation and strain localization failure of viscoplastic continua, Comput. Methods Appl. Mech. Engrg. 192 (2003) 955–971.
[22] M. Mabssout, M. Pastor, A two step Taylor–Galerkin algorithm for shock wave propagation in soils, Int. J. Numer. Anal. Methods Geomech. 27 (2003) 685–704.
[23] M. Mabssout, M. Pastor, M.I. Herreros, M. Quecedo, A. Runge-Kutta, Taylor–Galerkin scheme for hyperbolic systems with source terms. Application to shock wave propagation in viscoplastic geomaterials, Int. J. Numer. Anal. Methods Geomech. 30 (13) (2006) 1337–1355.
[24] J.J. Monaghan, R.A. Gingold, Shock simulation by the particle method SPH, J. Comput. Phys. 52 (1983) 374–389.
[25] J.J. Monaghan, J.C. Lattanzio, A refined particle method for astrophysical problems, Astron. Astrophys. 149 (1985) 135–143.
[26] J.J. Monaghan, Simulating free surface flows with SPH, J. Comput. Phys. 110 (1994) 399–406.
[27] J.J. Monaghan, Smoothed particle hydrodynamics, Rep. Prog. Phys. 68 (2005) 1703–1759.
[28] P. Perzyna, Fundamental Problems in Viscoplasticity, Recent Advances in Applied Mechanics, vol. 9, Academic Press, New York, 1966. pp. 243–377.
[29] T. Rabczuk, T. Belytschko, S.P. Xiao, Stable particle methods based on Lagrangian kernels, Comput. Methods Appl. Mech. Engrg. 193 (2004) 1035–1063.
[30] T. Rabczuk, T. Belytschko, A three dimensional large deformation meshfree method for arbitrary evolving cracks, Comput. Methods Appl. Mech. Engrg. 196 (29–30) (2007) 2777–2799.
[31] T. Rabczuk, J. Eibl, Simulation of high velocity concrete fragmentation using SPH/MLSPH, Int. J. Numer. Methods Engrg. 56 (2003) 1421–1444.
[32] P.W. Randles, L.D. Libersky, Smoothed particle hydrodynamics: some recent improvements and applications, Comput. Methods Appl. Mech. Engrg. 139 (1996) 375–408.
[33] P.W. Randles, L.D. Libersky, Normalized SPH with stress points, Int. J. Numer. Methods Engrg. 48 (2000) 1445–1462.
[34] J.A. Sethian, Level Set Methods and Fast Marching Methods, Cambridge University Press, Cambridge, 1999.